

The HI content of Fornax dwarf elliptical galaxies: FCC032 and FCC336

P. Buyle¹ ^{*}, S. De Rijcke¹ [†], D. Michielsen¹, M. Baes^{1,2}, H. Dejonghe¹

¹ *Sterrenkundig Observatorium, Universiteit Gent, Krijgslaan 281, S9, B-9000, Gent, Belgium*

² *European Southern Observatory, Casilla 19001, Santiago 19, Chile*

Accepted 1988 December 15. Received 1988 December 14; in original form 1988 October 11

ABSTRACT

We present HI 21 cm line observations, obtained with the Australia Telescope Compact Array, of two dwarf elliptical galaxies (dEs) in the Fornax cluster: FCC032 and FCC336. The optical positions and velocities of these galaxies place them well within the Fornax cluster. FCC032 was detected at the 3σ significance level with a total HI flux density of 0.66 ± 0.22 Jy km s⁻¹ or an HI mass of $5.0 \pm 1.7 \times 10^7 h_{75}^{-2} M_{\odot}$. Based on our deep H α + [NII] narrow-band images, obtained with FORS2 mounted on the VLT, this dE was already known to contain 600–1800 $h_{75}^{-2} M_{\odot}$ of ionised Hydrogen (depending on the relative strengths of the H α and [NII] emission lines). Hence, this is the first study of the complex, multi-phase interstellar medium of a dE outside the Local Group. FCC336 was detected at the same significance level: 0.37 ± 0.10 Jy km s⁻¹ or a total HI mass of $2.8 \pm 0.7 \times 10^7 h_{75}^{-2} M_{\odot}$. Using a compilation of HI data of dwarf galaxies, we find that the observed high HI-mass boundary of the distribution of dIrrs, BCDs, and dEs in a $\log(L_B)$ versus $\log(M_{HI})$ diagram is in good agreement with a simple chemical evolution model with continuous star formation. The existence of many gas-poor dEs (undetected at 21 cm) suggest that the environment (or more particularly, a galaxy’s orbit within a cluster) also plays a crucial role in determining the amount of gas in present-day dEs. E.g., FCC032 and FCC336 are located in the sparsely populated outskirts of the Fornax cluster. This is in agreement with HI surveys of dEs in the Virgo Cluster and an H α survey of the Fornax Cluster, which also tend to place gas-rich dwarf galaxies in the cluster periphery.

Key words: galaxies: individual: FCC032, FCC336 – galaxies: dwarf – galaxies: ISM – radio lines: galaxies

1 INTRODUCTION

One would not expect that dwarf elliptical galaxies (dEs) in dense environments contain a significant interstellar medium (ISM). Several arguments support this statement. Supernova-explosions are able to transfer enough energy to the ISM to heat it above the escape velocity in the least massive dwarfs (Mori et al. 1997). Alternatively, the frequent high-speed interactions with giant cluster-members to which a small late-type disk galaxy is subjected can transform it into a gasless spheroidal dE-like object. This “galaxy harassment” process (Moore et al. 1996) induces a dramatic morphological evolution on a time-span of about 3 Gyr. Moreover, hydrodynamical simulations of dwarf galaxies moving through the hot, thin intergalactic medium in clusters (Mori

& Burkert 2000; Michielsen, De Rijcke, Dejonghe 2004) or groups (Marcolini, Brighenti, D’Ercole 2003) show that ram-pressure stripping can completely remove the ISM of a dwarf galaxy less massive than $10^9 M_{\odot}$ within a few 100 Myrs. A quite different point of view on the origin of dEs comes to the same conclusion. If dEs are related to other dwarf galaxies such as Blue Compact Dwarfs (BCDs) or dwarf irregular galaxies (dIrrs), the “fading model” conjectures that star-forming dwarf galaxies will fade and reach an end-state similar to present-day dEs after they have used up their gas supply and star-formation has ended (Marlowe et al. 1999). Interactions may have sped up the gas-depletion process (van Zee, Skillman, Haynes 2004), explaining both the abundance of dEs and the paucity of BCDs/dIrrs in high-density environments.

For all these reasons, dEs in dense environments were generally thought to be virtually gas-depleted systems. However, evidence is building up that at least some dEs have retained part of their gas. In their multi-wavelength study

^{*} corresponding author: Pieter.Buyle@UGent.be

[†] Postdoctoral Fellow of the Fund for Scientific Research - Flanders (Belgium)(F.W.O)

of the Local Group dwarf galaxies, Young & Lo presented VLA HI observations of NGC147, NGC185, and NGC205 (Young & Lo 1996; Young & Lo 1997). These were the first observations that painted a detailed picture of the complex, multi-phase interstellar medium (ISM) of the most nearby representatives of the class of the dEs (Ferguson & Binggeli 1994). While NGC147 was not detected with a 3σ mass upper limit of $3 \times 10^3 M_\odot$ for an 8 km s^{-1} velocity width, NGC205 was found to contain $4.3 \times 10^5 M_\odot$ of neutral hydrogen and the total HI mass of NGC185 was estimated at $1.0 \times 10^5 M_\odot$. The neutral ISM of both detected galaxies turned out to be very clumpy, making a meaningful determination of their velocity fields rather difficult. Still, the stars and HI gas in NGC205 seem to have different rotation velocities while in NGC185, neither the HI or the stars show significant rotation (Simien & Prugniel 2002). Single-dish observations of ^{12}CO emission provide evidence that the molecular and atomic gas are kinematically linked. NGC205 was not detected on $\text{H}\alpha + [\text{NII}]$ narrow-band images while NGC185 contains an extended emission region, about 50 pc across (Young & Lo 1996; Young & Lo 1997).

More recently, HI surveys of the Virgo Cluster dE population (see Conselice et al. (2003) and references therein) have shown that roughly 15% of the dEs contain a neutral ISM. The detected HI masses range between 0.03 and $1.22 \times 10^9 M_\odot$. Processes that remove gas, such as galaxy interactions and ram-pressure stripping (Vollmer 2003; Marcolini, Brighenti, D’Ercole 2003; Michielsen, De Rijcke, Dejonghe 2004; Roediger & Hensler 2005), act most vigorously near the cluster center. Accordingly, the gas-rich dwarf galaxies in the Virgo cluster tend to have positions towards the outskirts of the cluster, suggesting that they are recent acquisitions of the cluster or are moving on orbits that avoid the cluster center. In a spectroscopic survey of the Fornax Cluster, Drinkwater et al. (2001) discovered $\text{H}\alpha$ emission in about 25% of the dEs. Again, most of these galaxies lie towards the outskirts of the cluster, while dEs near the center of the cluster are generally devoid of ionized gas.

In this paper, we present new HI 21 cm line observations of two dEs, obtained with the Australia Telescope Compact Array (ATCA). With optical systemic velocities $v_{\text{sys}} = 1318 \pm 26 \text{ km/s}$ (FCC032) and $v_{\text{sys}} = 1956 \pm 67 \text{ km/s}$ (FCC336) (Drinkwater et al. 2001), these dEs are bona fide members of the Fornax Cluster, located in the sparsely populated outskirts of the cluster (see Fig. 1). In section 2, we present our HI observations, followed by a discussion of our results in section 3. We summarize our conclusions in section 4.

2 HI OBSERVATIONS

We have used the Australia Telescope Compact Array on 20 and 23 December 2004 to observe two dEs in the Fornax cluster. We preferred interferometry observations above single-dish observations to avoid confusion with other galaxies that can be located within the large beam, which is a common nuisance in crowded environments such as the Fornax Cluster. The observations were made during night time to avoid solar RFI. We used the ATCA in the 1.5D configuration, with baselines ranging from 107 m to 4439 m. To be able to detect HI emission in three independent channels

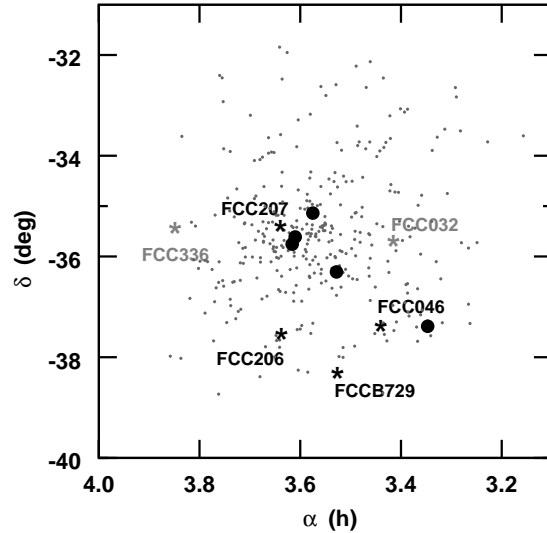


Figure 1. Positions of gas-rich dEs within the Fornax Cluster. Small dots indicate the positions of 340 galaxies in the Fornax Cluster Catalog. Large dots indicate the positions of galaxies brighter than $M_B < -20$ mag. Black asterisks indicate the positions of FCC046, FCC206, FCC207, and FCCB729. These dEs contain an ionised ISM (De Rijcke et al. (2003), Michielsen et al. (2004)). The positions of the HI detected Fornax dEs presented in this paper, FCC032 and FCC336, are indicated with a grey asterisk. FCC032 was detected both in $\text{H}\alpha$ and HI 21 cm emission.

and since both sources had an estimated velocity width of about 50 km s^{-1} , we selected a correlator setup that yielded 512 channels of width 15.6 kHz. To increase the signal-to-noise ratio the data were on-line Hanning smoothed which resulted in a velocity resolution of 6.6 km s^{-1} . At the start of each observation we observed the source 1934-638 as primary calibrator for 15 minutes. The source 0332-403 was observed every 40 minutes for 5 minutes as a secondary calibrator. The total integration time (including calibration) for each galaxy was 12h. The usual data reduction steps (phase, amplitude and bandpass calibration) were performed with the MIRIAD package (Sault et al. 1995), the standard ATCA data analysis program. We subtracted the continuum by performing a first order fit to the visibilities over the line-free channels which were not affected by the edge effects of the band (selected in advance by eye). The data cubes were created by using natural weighting and were subsequently smoothed with a Gaussian beam of $1' \times 1'$ (which corresponds to the optical spatial radius of our sources) and off-line Hanning smoothed to increase the signal-to-noise. The final data cubes had a spectral resolution of 13.3 km s^{-1} . Due to the faintness of these objects, we did not attempt a deconvolution of our images.

2.1 FCC032

FCC032 was selected as a suitable target because it was known to contain a sizable ionised ISM (Michielsen et al. 2004). This galaxy harbors a large ionised gas complex, about 850 pc across, containing star-formation regions and bubble-shaped gaseous filaments, probably supernova rem-

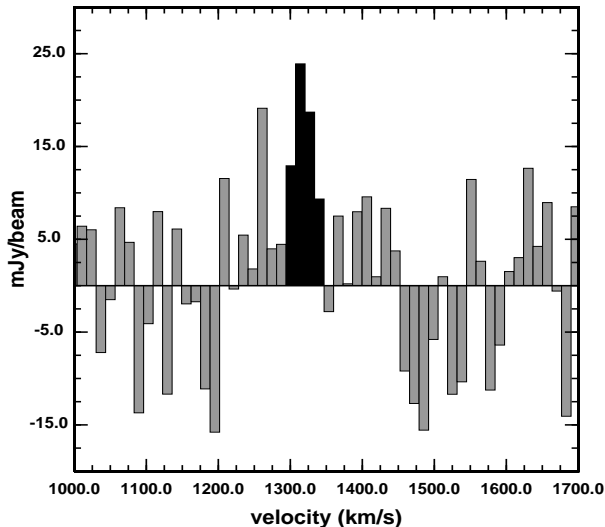


Figure 2. HI profile of FCC032, obtained by summing the flux within a $2' \times 2'$ box around the central radio position of the galaxy. The channels containing the 21 cm emission of FCC032 are colored in black.

nants. This offers strong evidence for recent or ongoing star formation in this dE.

Our final data cube had a synthesised beam of $87.56'' \times 55.55''$ due to the smoothing, resulting in a noise of 4 mJy/beam. These data cubes were inspected by eye for emission by plotting them over an optical image. The data were clipped at $1.5\sigma = 6$ mJy/beam. Weak emission near the optical center of the galaxy was found in 4 adjacent channels located around the optical systemic velocity. To derive a final spectrum (containing all detected HI), we summed the flux within a $2' \times 2'$ box centered on the central radio position of FCC032 which was derived from the total HI intensity map (see Fig.3). This resulted in a detection of the galaxy near the optical systemic velocity of 1318 km s^{-1} , spread over 4 channels (see Fig. 2).

We fitted a Gaussian to the global HI profile and adopted the method of Verheijen & Sancisi (2001) to measure the systemic velocity and line widths at the 20% and 50% levels (corrected for broadening and random motions). We applied the instrumental correction given by the formulae

$$W_{20} = W_{20,\text{obs}} - 35.8 \left[\sqrt{1 + (R/23.5)^2} - 1 \right], \quad (1)$$

$$W_{50} = W_{50,\text{obs}} - 23.5 \left[\sqrt{1 + (R/23.5)^2} - 1 \right], \quad (2)$$

with R the velocity resolution or 13.3 km s^{-1} in our case. This correction is based on approximating the edges of the global profile, which are mostly due to turbulent motion, with a Gaussian of dispersion 10 km s^{-1} . The results show a maximum flux of 24 mJy/beam at a velocity of 1318 km s^{-1} , which we adopt as the radio systemic velocity of FCC032 and which is in excellent agreement with the optically derived systemic velocity (Drinkwater et al. 2001). For the widths at 20% and 50% we found respectively 52 km s^{-1} and 34 km s^{-1} .

By summing the flux within the 4 channels that contain the 21 cm emission of FCC032, we created a total HI

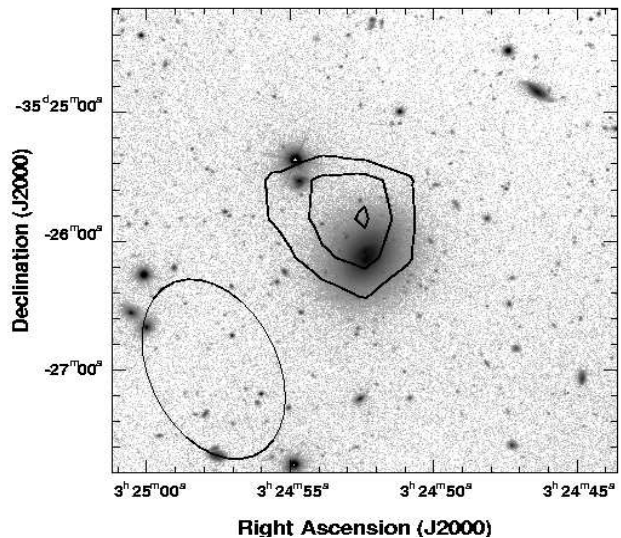


Figure 3. Total HI intensity map (contours) of FCC032 on top of an R-band grey-scale image (obtained with FORS2, VLT). The contours correspond to the $2\sigma_N^h$, $2.5\sigma_N^h$, and the $3\sigma_N^h$ levels with $\sigma_N^h = 0.11 \text{ Jy/beam km s}^{-1}$ (see eq. 3). The beam is plotted in the lower-left corner.

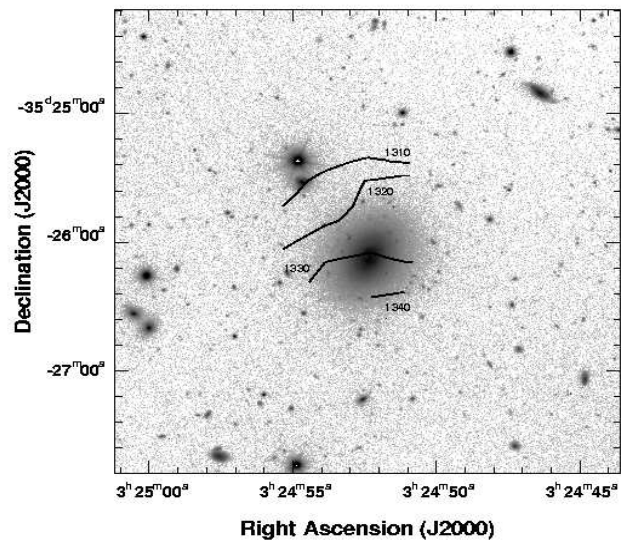


Figure 4. HI intensity-weighted velocity field of FCC032 (contours) on top of an R-band grey-scale image (obtained with FORS2, VLT). The contours are labeled with the velocity in km s^{-1} .

intensity map (see Fig. 3). The noise at a certain position in the total intensity map can be calculated by means of the formula (Verheijen & Sancisi 2001):

$$\sigma_N^h = \left(\frac{N}{2} - \frac{1}{8} \right)^{\frac{1}{2}} \frac{4}{\sqrt{6}} \sigma^h \quad (3)$$

where N stands for the number of channels that have been added at that position and with σ^h the noise in the Hanning smoothed channel maps (4 mJy/beam or $53.2 \text{ mJy/beam km s}^{-1}$). Not all channels contribute to the flux at a given position in the total intensity map so N is not the same everywhere. Typically, $N = 3$ in

this case. This yields an average spatial rms error $\sigma_N^h \approx 0.11 \text{ Jy/beam km s}^{-1}$. We rebinned the channels plotted in Fig. 2 by taking together 4 adjacent channels, such that all the 21 cm flux of FCC032 ends up in one single bin, 53.2 km s^{-1} wide, and then calculated the rms noise from the other bins. This way, we find a total velocity integrated HI flux density of $0.66 \pm 0.22 \text{ Jy km s}^{-1}$ and calculated a total estimated HI mass of $5.0 \pm 1.7 \times 10^7 h_{75}^{-2} M_\odot$, based on the W_{20} velocity width by means of the formula:

$$M_{\text{HI}} = 2.36 \times 10^5 D^2 \int S(v) dv M_\odot \quad (4)$$

with $D = 18 h_{75}^{-2} \text{ Mpc}$ the distance to the Fornax cluster and $\int S(v) dv$ the total flux density in units of Jy km s^{-1} . The HI intensity-weighted velocity field of FCC032 is presented in Fig. 4. A velocity gradient can be observed, suggesting rotation.

2.2 FCC336

FCC336 was selected according to its position in the outskirts of the Fornax cluster and thus, in accordance with the ram-pressure stripping theory, could be expected to harbor a relatively large amount of neutral hydrogen. Smoothing was again applied to the data cube to increase the signal-to-noise ratio, resulting in a synthesised beam of $110.60'' \times 82.13''$ and a noise of 4 mJy/beam . In a similar way as for FCC032, we found weak emission in three channels near the optical systemic velocity. We summed the flux within a $2' \times 2'$ box centered on the central radio position of the galaxy, which again was derived by the total HI intensity map, (see Fig. 6) in order to create a global HI profile of the galaxy. We found a strong intensity peak of 34.4 mJy/beam at a velocity of 2004 km s^{-1} (see Fig. 5), which is in fair agreement with the optical systemic velocity of $1956 \pm 67 \text{ km s}^{-1}$ (Drinkwater et al. 2001). A total HI intensity map shows that the emission, allowing for the coarse resolution of the HI map, coincides spatially with the optical image of the galaxy (see Fig. 6). We fit a Gaussian to the global HI profile and find a velocity width of 33 km s^{-1} and 22 km s^{-1} at respectively the 20% and 50% levels. We measure a total HI flux density of $0.37 \pm 0.10 \text{ Jy km s}^{-1}$, which, by means of formula (4), corresponds to an estimated total HI mass of $2.8 \pm 0.7 \times 10^7 h_{75}^{-2} M_\odot$. Here, we use the summed rms within the $2' \times 2'$ box and the W_{20} velocity width. Due to our velocity resolution of 13.3 km s^{-1} and the very small velocity width of FCC336, we did not attempt constructing an HI intensity-weighted velocity field.

3 DISCUSSION

In Fig. 7, we plot the B-band luminosities of FCC032 and FCC336 versus their HI masses, along with the Virgo dEs compiled by Conselice et al. (2003), the Local Group dEs NGC185 and NGC205 (Young & Lo 1996; Young & Lo 1997), the Local Group dwarf spheroidals (dSphs) and dwarf irregulars (dIrrs), taken from Mateo (1998), field dwarf irregulars and spheroidal galaxies, taken from Roberts et al. (2004), and Virgo Cluster Blue Compact Dwarfs (BCDs) and late-type dwarf galaxies (Sd-Sm-Im), taken from Gavazzi et al. (2005) and Sabatini et al. (2005). We

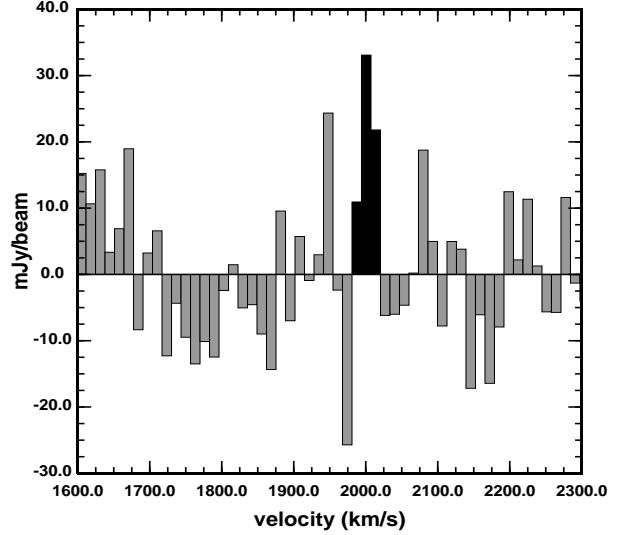


Figure 5. HI profile of FCC336, obtained by summing the flux within a $2' \times 2'$ box around the central radio position of the galaxy. The channels containing the 21 cm emission of FCC336 are colored in black.

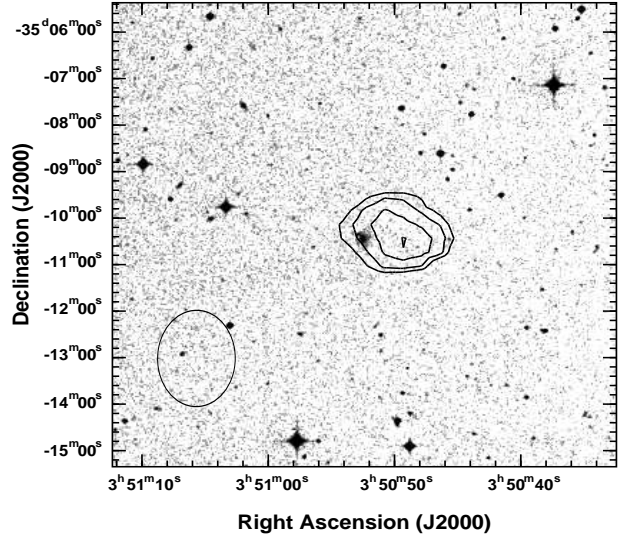


Figure 6. Total HI intensity map (contours) of FCC336 on top of an optical SDSS image (grey-scale). The contours correspond to the $2\sigma_N^h$, $2.5\sigma_N^h$, $3\sigma_N^h$, and $3.3\sigma_N^h$ levels, with $\sigma_N^h = 0.11 \text{ Jy/beam km s}^{-1}$ (see eq. 3). The beam is plotted in the bottom-left corner.

included only those galaxies in this diagram that were actually detected at 21 cm. Many dEs, however, are too gas-poor to have been detected in HI at the distances of the Virgo and Fornax clusters. HI studies in these clusters typically have mass-limits of the order of $10^7 M_\odot$. Only inside the Local Group have dEs and dSphs with a gas content as low as $\sim 10^5 M_\odot$ been detected. It should therefore be kept in mind that many dEs reside in the upper left part of this figure that have so far evaded detection.

Clearly, BCDs and dIrrs seem to trace a sequence, defined roughly by the relation $\log(L_B) \approx \log(M_{\text{HI}})$. All these galaxies reside either in the Virgo cluster or in the Local

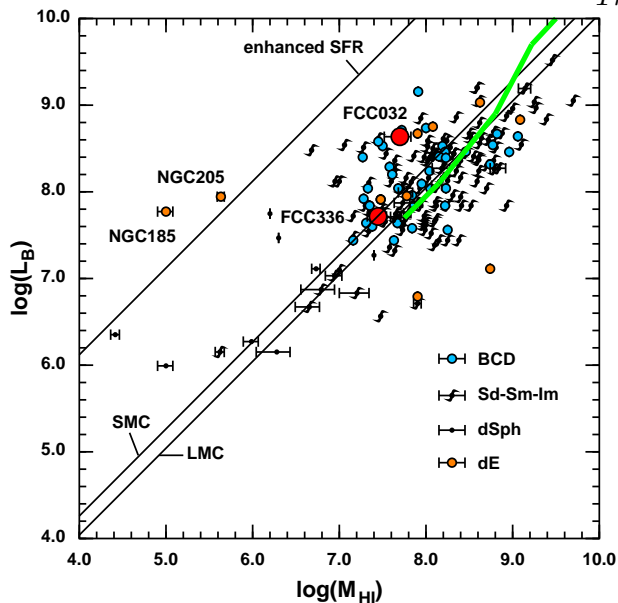


Figure 7. B-band luminosity (in $L_{\odot,B}$) versus HI mass (in M_{\odot}). Large white circles indicate FCC032 and FCC336; small white circles correspond to Virgo dwarf ellipticals, except for the two leftmost white circles, which are NGC185 and NGC205. The small grey dots are Virgo Cluster BCDs. Late-type dwarfs (Sd-Sm-Im) in the Local Group, the Virgo Cluster and in the field are indicated by spiral symbols. Black dots correspond to Local group and field dwarf spheroidals. The full lines trace the sequences predicted by simple chemical evolution models for various star-formation efficiencies; the grey curve traces the $\log(L_B)$ vs. $\log(M_{\text{HI}})$ relation of late-type galaxies predicted by semi-analytical models of galaxy formation via hierarchical merging in a Λ CDM universe (see section 3). We stress the fact that only detected galaxies have been included in this figure. Many dEs, however, are too gas-poor to have been detected in HI at the distances of the Virgo and Fornax clusters. HI studies in these clusters typically have mass-limits of the order of $10^7 M_{\odot}$. Only inside the Local Group have dEs and dSphs with a gas content as low as $\sim 10^5 M_{\odot}$ been detected. It should therefore be kept in mind that many dEs reside in the upper left part of this figure but have not yet been detected.

group, with secure distance estimates (Mateo 1998). This makes us confident that this sequence is not a spurious result of the distance-dependence of both $\log(L_B)$ and $\log(M_{\text{HI}})$. The Local Group dSphs and the Local Group dEs NGC185 and NGC205 (both are satellites of M31) deviate from this sequence by being gas deficient. Non-detections at 21 cm were not plotted in this figure. Hence, many undetected gas-poor dwarf galaxies (like NGC147, with a 3σ upper limit of $3 \times 10^3 M_{\odot}$ for M_{HI} (Young & Lo, 1997), or the 20 Virgo dEs that were not detected by Conselice et al. (2003), with mass upper limits of $\sim 8 \times 10^6 M_{\odot}$) are expected to occupy the left part of the diagram. Therefore, the L_B vs. M_{HI} sequence of gas-rich dwarf galaxies in Fig. 7 is best seen as a boundary, enclosing the most HI-rich galaxies while many gas-poor dwarfs (like dEs and dSphs) lie significantly to the left of this sequence.

3.1 Chemical evolution of dwarf galaxies

In order to interpret this diagram, we overplotted the observed data points with theoretical predictions for the

$\log(L_B)$ vs. $\log(M_{\text{HI}})$ relation, based on the analytical models of Pagel & Tautvaišienė (1998) for the chemical evolution of the Large and Small Magellanic Clouds. In the formalism of these models, galaxies are formed by the infall of pristine gas. Stars are born at a rate proportional to the gas mass and supernova explosions eject gas at a rate proportional to the star-formation rate (SFR). The build-up of the elemental abundances is calculated using the delayed-recycling approximation in order to include the contribution of SNIa. We used the B-band mass-to-light ratios of single-age t , single-metallicity Z stellar populations (or SSPs), denoted by $\Upsilon_B^*(Z, t)$, presented by Vazdekis et al. (1996), in order to calculate the present-day L_B/M_{HI} ratio as

$$\frac{L_B}{M_{\text{HI}}}(T) = \frac{1}{g(T)} \int_0^T \frac{\omega g(T-t)}{\Upsilon_B^*(Z(T-t), t)} dt \quad (5)$$

with $T = 13 \text{ Gyr}$ the assumed age of the galaxies, $g(t)$ the gas mass at time t , and ω the star-formation efficiency (or the inverse time-scale for star formation). The time-dependence of g and Z is taken from Pagel & Tautvaišienė (1998) (their equations (6), (8), (11), and (14)). The rightmost curve in Fig. 7, labeled with “LMC”, corresponds to parameter values fine-tuned to reproduce the elemental abundances observed in the LMC (star-formation efficiency $\omega = 0.18 \text{ Gyr}^{-1}$ and outflow parameter $\eta = 1$); the middle curve, labeled with “SMC”, corresponds to the SMC (star-formation efficiency $\omega = 0.115 \text{ Gyr}^{-1}$ and outflow parameter $\eta = 2$). Clearly, these simple models nicely reproduce the observed locus of the gas-rich dwarf late types, BCDs, and dEs. The green curve in Fig. 7 traces the $\log(L_B)$ vs. $\log(M_{\text{HI}})$ relation of late-type galaxies predicted by semi-analytical models (SAMs) of galaxy formation via hierarchical merging in a Λ CDM universe (Nagashima & Yoshii 2004). SAMs make use of a Monte-Carlo technique to construct the hierarchical merger tree that leads up to the formation of a galaxy of a given mass. They moreover contain prescriptions for star-formation, energy feedback from supernova explosions, gas cooling, tidal stripping, dust extinction, and the dynamical response to starburst-induced gas ejection. Despite the inevitable oversimplifications in the description of immensely complex processes such as star formation, they are able to account pretty well for many observed properties of galaxies. The green curve in Fig. 7 indicates the amount of cold gas present in simulated galaxies that were classified as late-types (see also Fig. 4 in Nagashima & Yoshii, 2004).

Thus, it seems that the locus of gas-rich Sd-Sm-Im galaxies and BCDs in Fig. 7 can be reproduced quite satisfactorily by chemical evolution models of isolated galaxies in which slow star formation does not exhaust all available gas within a Hubble time.

3.1.1 Enhanced star-formation rate

Using the same formalism, one can produce more gas-poor systems by raising the star-formation efficiency ω . For instance, interactions may have sped up the gas-depletion process (van Zee, Skillman, Haynes 2004; Sabatini et al. 2005), explaining both the abundance of gas-poor dEs and the paucity of gas-rich BCDs/dIrrs in high-density environments. E.g., the leftmost curve in Fig. 7, labeled with “enhanced SFR”, corresponds to a model with a star-formation

efficiency that is a factor of 3 higher than in the LMC model (star-formation efficiency $\omega = 0.54 \text{ Gyr}^{-1}$ and outflow parameter $\eta = 1$). This way, one can reproduce the locus of gas-poor dwarf galaxies such as the Local Group dwarf dSphs. All models presented in Fig. 7 have luminosity-weighted mean metallicities in the range $[\text{Fe}/\text{H}] = -0.65$ to -0.4 . The models with a high SFR consume their gas reservoir in a strong starburst at an early epoch, when the gas was not yet enriched with metals, and hence, even though they form stars more efficiently, do not have significantly higher mean metallicities than the low SFR models (although they do contain a sprinkling of recently formed metalrich stars which are absent in low SFR models). As discussed in Grebel et al. (2003), dSphs indeed have more metalrich red giants than dIrrs and show evidence for a more vigorous early enrichment than dIrrs.

3.1.2 Enhanced gas-ejection efficiency

Raising the gas-ejection efficiency can also enhance the L_B/M_{HI} ratio although, at the same time, it significantly lowers the mean metallicity by effectively terminating further star-formation after the first star-forming event (e.g. making the gas-ejection by supernovae 30 times as efficient as in the Magellanic Clouds leads to $L_B/M_{\text{HI}} \approx 3.3$ and $[\text{Fe}/\text{H}] \approx -1.6$). However, the star-formation histories of the Local Group dSphs seem rather continuous (with the exception of the Carina dSph) and show no evidence for major starbursts which would be able to expell significant amounts of gas (Grebel 2000). On the other hand, as argued by Ferrara & Tolstoy (2000), MacLow & Ferrara (1999), and De Young & Heckman (1994), a centralised star-burst event in a round galaxy is much more efficient at transferring energy to the ISM (and hence at expelling gas out of a galaxy) than a similar star-burst in a disk galaxy since, in the latter case, the hot supernova-driven gas can break through the disk galaxy along the minor axis. Hence, this suggests that rotationally flattened galaxies, such as dwarf late-types, indeed have lower gas-ejection efficiencies than dEs and dSphs. The metallicity-flattening relation observed in dEs (Barazza & Binggeli 2002), with more flattened dEs tending to be less metal-rich, seems to indicate that in flattened dEs, individual supernova-explosions or star-formation sites are better able to eject the hot, enriched gas via a chimney perpendicular to the disk, without appreciably affecting the surrounding ISM, than in round dEs. This leads to flattening as a second parameter in controlling a dE's metallicity besides total mass.

3.1.3 External gas-removal mechanisms

Hydrodynamical simulations of dwarf galaxies moving through the hot, rarefied intracluster medium show that ram-pressure stripping can completely remove the ISM of a low-mass dwarf galaxy (Mori & Burkert 2000; Vollmer 2003; Marcolini, Brighenti, D'Ercole 2003; Michielsen, De Rijcke, Dejonghe 2004). Interactions and ram-pressure stripping are most efficient at removing gas from galaxies near the cluster center. Indeed, the gas-rich dwarf galaxies in the Virgo cluster tend to have positions towards the outskirts of the cluster (e.g. Conselice et al. (2003)), suggesting that they

are recent acquisitions of the cluster or are moving on orbits that avoid the cluster center. In a spectroscopic survey of the Fornax Cluster, Drinkwater et al. (2001) discovered $\text{H}\alpha$ emission in about 25% of the dEs. Again, most of these galaxies lie towards the cluster periphery, while dEs near the center of the cluster are generally devoid of ionized gas. Likewise, both HI -rich dEs presented in this paper are located in the sparsely populated outskirts of the Fornax cluster (see Fig. 1).

4 CONCLUSIONS

Based on our HI 21 cm observations of dEs in the Fornax Cluster and on HI 21 cm observations of dEs, BCDs, and late-type dwarf galaxies in the Virgo Cluster (Conselice et al. 2003; Gavazzi et al. 2005), and the Local Group dwarfs (Mateo 1998), we conclude that the gas-content of the most gas-rich dwarf galaxies is consistent with a continuous, slow star-formation history. After one Hubble time, these galaxies still have a large gas reservoir left and roughly trace a sequence defined by the relation $\log(L_B) \approx \log(M_{\text{HI}})$. However, the majority of the dwarf spheroidals and dwarf ellipticals contain significantly less gas than predicted by this relation. External gas-removal mechanisms such as a star-formation rate enhanced by gravitational interactions or ram-pressure stripping can account very well for the existence of these gas-poor systems. Such external mechanisms will act most vigorously in high-density environments, offering a natural explanation for the trend for HI mass to increase with distance from the nearest massive galaxy (Grebel 2000), and the fact that gas-rich dEs are observed predominantly in the outskirts of clusters.

ACKNOWLEDGMENTS

We wish to thank C. De Breuck for his kind help and advice and the anonymous referee for the very helpful suggestions. DM and BP wish to thank the Bijzonder Onderzoeksfonds (BOF) of Ghent University for financial support. This paper is based on data obtained with the Australia Telescope Compact Array (ATCA). The Australia Telescope is funded by the Commonwealth of Australia for operation as a National Facility managed by CSIRO. This research has made use of the NASA/IPAC Extragalactic Database (NED) which is operated by the Jet Propulsion Laboratory, California Institute of Technology, under contract with the National Aeronautics and Space Administration.

REFERENCES

- Barazza, F. D. & Binggeli, B., 2002, *A&A*, 394, L15
- Conselice, C., O'Neil, K., Gallagher, J. S., Wyse, R. F. G., 2003, *ApJ*, 591, 167
- De Young, D. S. & Heckman, T. M., 1994, *ApJ*, 431, 598
- De Rijcke, S., Zeilinger, W. W., Dejonghe, H., Hau, G. K. T., 2003, *MNRAS*, 339, 225
- Drinkwater, M. J., Gregg, M. D., Holman, B. A. & Brown, M. J. I., 2001, *MNRAS*, 326, 1076
- Ferguson, H. C. & Binggeli, B., 1994, *A&ARv*, 6, 67
- Ferrara, A. & Tolstoy, E., 2000, *MNRAS*, 313, 291

- Gavazzi, G., Boselli, A., van Driel, W., O'Neil, K., 2005, *A&A*, 429, 439
- Grebel, E. K., 2000, in "Star formation from the small to the large scale", ESLAB symposium. Eds.: F. Favata, A. Kaas, and A. Wilson, p. 87
- Grebel, E. K., Gallagher III, J. S., Harbeck, D., 2003, *ApJ*, 125, 1926
- MacLow, M. & Ferrara, A., 1999, *ApJ*, 513, 142
- Marcolini, A., Brighenti, F., D'Ercole, A., 2003, *MNRAS*, 345, 1329
- Marlowe, A. T., Meurer, G. R., Heckman, T. M., 1999, *ApJ*, 522, 183
- Mateo, M. L., 1998, *ARA&A*, 36, 435
- Michielsen, D., De Rijcke, S., Zeilinger, W. W., Prugniel, P., Dejonghe, H., Roberts, S., 2004, *MNRAS*, 353, 1293
- Michielsen, D., De Rijcke, S., Dejonghe, H., 2004, *ANS*, 325, 122
- Moore B., Katz N., Lake G., Dressler A., Oemler A., Jr., 1996, *Nature*, 379, 613
- Mori M. & Burkert A., 2000, *ApJ*, 538, 559
- Mori, M., Yoshii, Y., Tsujimoto, T., Nomoto, K., 1997, *ApJ*, 479, L21
- Nagashima, M. & Yoshii, Y., 2004, *ApJ*, 610, 23
- Pagel, B. E. J., Tautvaišienė, G., 1998, *MNRAS*, 299, 535
- Roberts, S., Davies, J., Sabatini, S., van Driel, W., O'Neil, K., Baes, M., Linder, S., Smith, R., Evans, R., 2004, *MNRAS*, 352, 478
- Roediger, E. & Hensler, G., accepted by *A&A*, astro-ph/0412518
- Sabatini, S., Davies, J., van Driel, W., Baes, M., Roberts, S., Smith, R., Linder, S., O'Neil, K., 2005, *MNRAS*, 357, 819
- Sault, R.J., Teuben, P.J., Wright, M.C.H., 1995, in Shaw R., Payne H.E., Hayes J.J.E., eds, *ASP Conf. Ser. Vol. 77, Astronomical Data Analysis Software and Systems IV*. Astron. Soc. Pac., San Francisco, p.433
- Simien, F. & Prugniel, Ph., 2002, *A&A*, 384, 371
- Tully, R.B. & Fouque, P., 1985, *ApJS*, 58, 67
- van Zee, L., Skillman, E. D., Haynes, M. P., 2004, *AJ*, 128, 121
- Vazdekis, A., Casuso, E., Peletier, R. F., Beckman, J. E., 1996, *ApJS*, 106, 307
- Verheijen, M.A.W. & Sancisi, R., 2001, *A&A*, 370, 765
- Vollmer, B., 2003, *A&A*, 398, 525
- Young, L. M. & Lo, K. Y., 1997, *ApJ*, 476, 127
- Young, L. M. & Lo, K. Y., 1996, *ApJ*, 464, L59

This paper has been produced using the Royal Astronomical Society/Blackwell Science L^AT_EX style file.